Productions of second Kaluza-Klein gauge bosons in the minimal universal extra dimension model at LHC

Shigeki Matsumoto,[1,*] Joe Sato,[2,†] Masato Senami,[3,‡] and Masato Yamanaka[2,§]

[1]*Department of Physics, University of Toyama, Toyama 930-8555, Japan*
[2]*Department of Physics, Saitama University, Shimo-okubo, Sakura-ku, Saitama, 338-8570, Japan*
[3]*Department of Micro Engineering, Kyoto University, Kyoto 606-8501, Japan*

(Received 18 March 2009; revised manuscript received 3 August 2009; published 25 September 2009)

We calculate the production rates of the second Kaluza-Klein (KK) photon $\gamma^{(2)}$ and Z boson $Z^{(2)}$ at the LHC including all significant processes in the minimal universal extra dimension (MUED) model. For discrimination of the MUED model from other TeV scale models at the LHC, $\gamma^{(2)}$ and $Z^{(2)}$ play a crucial role. In order to discuss the discrimination and calculate their production rates, we derive KK number violating operators including the contribution of the top Yukawa coupling. Using these operators, we accurately calculate branching ratios of second KK particles. In addition we find that these KK number violating operators provide new processes for $\gamma^{(2)}$ and $Z^{(2)}$ productions, such as cascade decay from second KK quarks produced through these operators. They have large contributions to their total production rates. In particular, these production processes give the dominant contribution for $\gamma^{(2)}$ production for $1/R \gtrsim 800$ GeV. As a result, with an integrated luminosity of 100 fb^{-1}, the number of produced $\gamma^{(2)}$ and $Z^{(2)}$ are estimated as 10^6–10^2 for the compactification scale between 400 and 2000 GeV.

DOI: 10.1103/PhysRevD.80.056006 PACS numbers: 11.10.Kk, 12.60.−i

I. INTRODUCTION

Theoretical arguments in particle physics and cosmological observations conclude that the standard model (SM) is not the theory of everything but is rather the effective theory describing physics below $\mathcal{O}(100)$ GeV. Many models beyond the SM have been proposed, and the universal extra dimension (UED) models [1] are some of the attractive candidates for new physics at TeV scale.[1] In the UED models, all SM fields can propagate into compactified extra dimensions, and hence they are accompanied by the tower of Kaluza-Klein (KK) particles. They can give plausible explanations for the existence of dark matter [3], the number of fermion generations [4], SM neutrino masses which are embedded in extended models [5], and so on. Among various UED models, the simplest and the most popular one is called the minimal UED (MUED) model. The MUED model is defined on the five-dimensional space-time, where the extra dimension is compactified on an S^1/Z_2 orbifold. In the MUED model, only two parameters are newly introduced to the SM. One is the compactification scale of the extra dimension $1/R$, the inverse of the radius of S^1 circle, and the other is the cutoff scale of the MUED model Λ. In order to satisfy terrestrial experiments, $1/R$ must be larger than 400 GeV [1,6], while the calculation of the relic abundance of the lightest KK particle (LKP) suggests that the abundance of the dark matter is explained for $500\ \text{GeV} \lesssim 1/R \lesssim 1500\ \text{GeV}$ [7]. As indicated from these results, the MUED model would be discovered and studied at the Large Hadron Collider (LHC).

The confirmation of the MUED model (in general, UED models) at collider experiments requires the discovery of KK particles. Though the LHC can produce KK particles, it is difficult to confirm that they are indeed the KK particles, because new particles predicted in various TeV scale models give quite similar signatures to each other. Therefore it is very important to understand how they can be identified as KK particles. In this article, we discuss the discrimination of the MUED model from other TeV scale models.

In Ref. [8], an excellent idea to discriminate the MUED model from other TeV scale models has been proposed. The essence of the discrimination is the discovery of the second KK particles. The signals of the first KK particles are quite similar to those of new particles in other models. However, the discovery of the second KK particles strongly suggests the existence of the MUED model, since their masses are peculiarly almost equal to $2/R$, and the value of $1/R$ is expected by the masses of the ''first KK'' particles. In particular, the second KK photon $\gamma^{(2)}$ and Z boson $Z^{(2)}$ play an important role for the search of the second KK particles. They are able to decay into two charged leptons. It is possible to reconstruct the masses of $\gamma^{(2)}$ and $Z^{(2)}$ clearly from the charged dileptons emitted by them. Connecting their masses and those of the first KK particles, we can confirm the realization of the MUED model.

Hence, $\gamma^{(2)}$ and $Z^{(2)}$ are the key ingredients to discriminate the MUED model from other TeV scale models. We

*smatsu@sci.u-toyama.ac.jp
†joe@phy.saitama-u.ac.jp
‡senami@me.kyoto-u.ac.jp
§masa@krishna.phy.saitama-u.ac.jp

[1]UED models are motivated by the TeV scale extra dimension theory [2].

 © 2009 The American Physical Society

therefore calculate their production rates at the LHC. To do this, first we derive the effective Lagrangian containing KK number violating operators, which are relevant to both the second KK particles productions and decay. Previously, these operators have been discussed in Ref. [9] considering only gauge interactions. We improve the operators by including the contribution of Yukawa interactions. Through the KK number violation operators, $\gamma^{(2)}$ and $Z^{(2)}$ decay into dilepton. In addition to the decay, these operators allow single second KK particle production, which does not suffer from a severe kinematical suppression compared to pair productions. Next we study the production processes of $\gamma^{(2)}$ and $Z^{(2)}$ including both the KK number violating and conserving processes. At the LHC, $\gamma^{(2)}$ and $Z^{(2)}$ are produced mainly through the cascade decays of the second KK gluons $g^{(2)}$ and quarks $q^{(2)}$. Here the symbol q stands for both $SU(2)$ doublet and singlet quarks. We also need to calculate their branching ratios into $\gamma^{(2)}$ and $Z^{(2)}$. Finally, we calculate the production rates of $\gamma^{(2)}$ and $Z^{(2)}$ from each process, and estimate the number of the dilepton signals from them.

This article is organized as follows. In the next section, we briefly review the MUED model. Then we mention the difficulty that appears during the confirmation of the MUED model at the LHC, and discuss an idea to overcome the difficulty. In Sec. III, we discuss the Lagrangian relevant to the productions of $\gamma^{(2)}$ and $Z^{(2)}$, and we calculate the branching ratios of colored second KK particles. In Sec. IV, we show some numerical results for $\gamma^{(2)}$ and $Z^{(2)}$ productions, and discuss the significance to discover the particles at the LHC. Section V is devoted to summary.

II. THE MUED MODEL AND ITS DISCRIMINATION FROM OTHER MODELS

The MUED model is the simplest version of the UED models. In this model, fields with a fifth dimensional momentum n/R behave as new heavy particles with a tree-level mass $\sqrt{m_{\rm SM}^2 + (n/R)^2}$ from the viewpoint of four-dimensional field theory. These new particles are called KK particles, n is called the KK number ($n = 0$ for SM particles, $n = 1, 2, \ldots$ for KK particles), and $m_{\rm SM}$ represents the mass of the corresponding SM particle.

The SM particles and their KK particles have identical gauge charges and spins. All interactions of the KK particles in the four-dimensional space-time are determined by the Lagrangian in five dimensions. Since the UED models are not renormalizable, they should be considered as an effective theory defined at the scale Λ, where Λ is usually taken to be $\Lambda R \sim \mathcal{O}(10)$ [1,10]. In this article, we take Λ to be $\Lambda R = 20$.[2] Thus, in order to discuss the phenomenology of the MUED model, we need only two new parameters: $1/R$ and Λ.

Although the masses of KK particles at tree level are highly degenerate in each KK mode, the degeneracy is slightly relaxed by radiative corrections [9]. The mass spectrum of the nth KK particles with the radiative corrections δm_n are given by $m_n = \sqrt{(n/R)^2 + m_{\rm SM}^2 + \delta m_n^2}$. Here, analytical expressions of the radiative corrections δm_n are given in Ref. [9]. In general, due to the radiative corrections, colored KK particles are heavier than non-colored KK particles in each KK level. We have used couplings improved by the renormalization group (RG) equation to compute the radiative corrections to the masses of KK particles. The gauge couplings at the one-loop level are given by

$$\alpha_i^{-1}(\mu) = \alpha_i^{-1}(m_Z) - \frac{b_i}{2\pi}\ln[\mu/m_Z] - \sum_n \theta(\mu - n/R)\frac{\tilde{b}_i}{2\pi}\ln[\mu/(n/R)]. \quad (1)$$

Here $\alpha_i = g_i^2/(4\pi)$, $g_i = (g', g_2, g_s)$ are the SM gauge coupling constants (i stands for each gauge group), μ is the renormalization scale, and θ represents the step function. b_i and $\tilde{b}_i$ are summarized in Table I.

The mass spectrum of the first KK particles ($n = 1$) and the second KK particles ($n = 2$) for $1/R = 500$ GeV are shown in Table II. When we calculate the mass spectrum of nth KK particles, we choose their mass scale, n/R, as renormalization scale. It is seen that each KK mode is degenerate with each other and the masses of the second KK particles are almost twice of the first KK particles.

Since the translational invariance along the extra dimension direction is broken due to the orbifolding on an S^1/Z_2, the fifth dimensional momentum (KK number) is no longer conserved. Nevertheless, the subgroup of the translational invariance remains unbroken, which is called the KK parity. Under the parity, particles with even (odd) KK number have plus (minus) sign, and the product of the sign is conserved in each process. Because of the KK parity conservation, the lightest KK particle (LKP) is stable and provided as a candidate for dark matter. The situation is quite similar to the case of supersymmetric models with R-parity conservation, in which the lightest supersymmetric particle (LSP) is stable. The relic abundance of the KK particle dark matter has been calculated in the MUED

TABLE I. Coefficients of RG improved gauge coupling constants. Each $\tilde{b}_i$ is the contribution from one KK level of KK particles.

Fields	b'	b_2	b_s	$\tilde{b}'$	$\tilde{b}_2$	$\tilde{b}_s$
Gauge	0	$-22/3$	-11	0	-7	$-21/2$
Higgs	$1/6$	$1/6$	0	$1/6$	$1/6$	0
Fermion	$20/3$	4	4	$40/3$	8	8

[2]Our results are almost independent of Λ, since it always appears with a loop suppression and gives only logarithmic corrections.

TABLE II. Mass spectrum of KK particles for $1/R = 500$ GeV and $\Lambda R = 20$.

KK particle	$n = 1$	$n = 2$
KK gluon $g^{(n)}$	618 GeV	1170 GeV
KK Z boson $Z^{(n)}$	534 GeV	1059 GeV
KK W boson $W^{\pm(n)}$	534 GeV	1046 GeV
KK photon $\gamma^{(n)}$	501 GeV	1000 GeV
KK Higgs $H^{(n)}$	518 GeV	1014 GeV
KK CP-odd Higgs $A^{(n)}$	512 GeV	1011 GeV
KK charged Higgs $H^{\pm(n)}$	510 GeV	1010 GeV
KK $SU(2)$ singlet electron $E^{(n)}$	505 GeV	1008 GeV
KK $SU(2)$ doublet lepton $L^{(n)}$	514 GeV	1022 GeV
KK $SU(2)$ singlet up quark $U^{(n)}$	571 GeV	1100 GeV
KK $SU(2)$ singlet down quark $D^{(n)}$	569 GeV	1097 GeV
KK $SU(2)$ doublet quark $Q^{(n)}$	582 GeV	1117 GeV
KK light top quark $T^{(n)}$	569 GeV	1071 GeV
KK heavy top quark $t^{(n)}$	594 GeV	1109 GeV
KK $SU(2)$ singlet bottom quark $B^{(n)}$	569 GeV	1097 GeV
KK $SU(2)$ doublet bottom quark $b^{(n)}$	575 GeV	1106 GeV

model [7], and it turns out that if the KK particle dark matter dominates the component of dark matter in the universe, $1/R$ should be in the range of 500–1500 GeV. The MUED model, therefore, would be explored at the LHC.

The confirmation of the MUED model at the LHC is not so easy. Although it is necessary to discover the KK particles, it is very hard to distinguish the signals of these particles from those of other TeV scale models (for example, the minimal supersymmetric standard model, the little Higgs models, and so on), because these models also predict new heavy particles which give quite similar signals. For example, in a supersymmetric model, new particles also have identical couplings to their corresponding SM particles and the masses of colored new particles are heavier than those of other new particles. Furthermore, there is a conserved discrete symmetry (R parity), which makes LSP stable. In both models, at the LHC, heavy colored new particles are produced first. Then they immediately decay into lighter new particles. Finally the lightest new particles leave detectors as missing energy. The spin difference may be used to discriminate the MUED model from other models [11]. However, the spin determination, particularly when the masses of new particles are degenerate, is difficult at the LHC, and hence the discrimination of TeV scale models is also difficult.

In order to discriminate the signals of the MUED model from those of other models, we focus on the existence of the KK tower. First of all, we need to speculate the value of $1/R$. At the LHC, we can find the signals of first KK particles through the four lepton channel [12]. Through the observations of cascade decays of the first KK particles, we can speculate the value of $1/R$. It is then possible to predict the masses of the second KK particles. The discovery of new particles with predicted masses strongly suggests that the MUED model is realized as new physics at the TeV scale. At tree level, the second KK particles decay into lighter KK particles through KK number conserving processes, and eventually LKPs are left. Since the LKP gives no signal at the detectors, it is very hard to measure the mass of its parent particle. Fortunately, the second KK gauge bosons directly couple with SM fermion pairs through KK number violating interactions. Consequently, $\gamma^{(2)}$ and $Z^{(2)}$ decay into two charged leptons with nonzero branching ratios, and the masses of $\gamma^{(2)}$ and $Z^{(2)}$ can be clearly reconstructed from the dileptons [8]. The mass difference between $\gamma^{(2)}$ and $Z^{(2)}$ is about 50 GeV for $1/R = 500$ GeV, as shown in Table I, and for this mass difference each resonance can be distinguished clearly by the observation of dielectron signals [8]. The double peak resonance also suggests the existence of the MUED model, because this is one of the typical signatures of this model. For the discussion of the feasibility to confirm the MUED model at the LHC, we need to know the event rate of the dilepton signals. We thus calculate the production rates of $\gamma^{(2)}$ and $Z^{(2)}$ at the LHC in the following sections.

III. PRODUCTIONS OF $\gamma^{(2)}$ AND $Z^{(2)}$

In this section, we discuss the Lagrangian relevant to the production of $\gamma^{(2)}$ and $Z^{(2)}$ bosons. With the Lagrangian we calculate the branching ratios of $g^{(2)}$ and $q^{(2)}$, which are necessary for the discussion of the indirect production of $\gamma^{(2)}$ and $Z^{(2)}$.

A. Lagrangian for $\gamma^{(2)}$ and $Z^{(2)}$ productions

First, we show the Lagrangian conserving the KK number relevant to gauge bosons,

$$\begin{aligned}\mathcal{L}_{\rm con} = & -g_i \sum_{n=1}^{\infty} [\bar{f}^{(n)} t^a \gamma^\mu f^{(n)} V_{i\mu}^{(0)a} + \bar{f}^{(n)} t^a \gamma^\mu P_{L(R)} f^{(0)} V_{i\mu}^{(n)a} + \bar{f}^{(0)} t^a \gamma^\mu P_{L(R)} f^{(n)} V_{i\mu}^{(n)a}] \\ & - \frac{g_i}{\sqrt{2}} \sum_{n,m=1}^{\infty} [\bar{f}^{(n)} t^a \gamma^\mu \gamma^5 f^{(m)} V_{i\mu}^{(n+m)a} + \bar{f}^{(n+m)} t^a \gamma^\mu f^{(n)} V_{i\mu}^{(m)a} + \bar{f}^{(n)} t^a \gamma^\mu f^{(n+m)} V_{i\mu}^{(m)a}] \\ & + g_i f_i^{abc} \sum_{n=1}^{\infty} [(\partial_\mu V_{i\nu}^{(0)a}) V_i^{(n)b\mu} V_i^{(n)c\nu} + (\partial_\mu V_{i\nu}^{(n)a}) V_i^{(n)b\mu} V_i^{(0)c\nu} + (\partial_\mu V_{i\nu}^{(n)a}) V_i^{(0)b\mu} V_i^{(n)c\nu}], \end{aligned} \tag{2}$$

where the summation over i, a, b, and c is implicitly made. $f^{(n)}$, g_i, t^a, and $V_{i\mu}^a$ are listed in Table III. In the third part of the

TABLE III. $f^{(n)}$, g_i, t^a, and $V^a_{i\mu}$ in the KK number conserving Lagrangian. B, W, and g are $U(1)$, $SU(2)$, and $SU(3)$ gauge bosons, g', g_2, and g_s are $U(1)$, $SU(2)$, and $SU(3)$ gauge coupling constants, and σ^a and λ^a are Pauli matrices and Gell-Mann matrices, respectively.

nth KK fermion $f^{(n)}$	g_i	t^a	$V^a_{i\mu}$
$SU(2)$-singlet charged lepton $E^{(n)}$	$-g'$	1	B_μ
$SU(2)$-doublet lepton $L^{(n)}$	$-(1/2)g'$	1	B_μ
	g_2	$\sigma^a/2$	W^a_μ
$SU(2)$-singlet up-type quark $U^{(n)}$	$(2/3)g'$	1	B_μ
	g_s	$\lambda^a/2$	g^a_μ
$SU(2)$-singlet down-type quark $D^{(n)}$	$-(1/3)g'$	1	B_μ
	g_s	$\lambda^a/2$	g^a_μ
$SU(2)$-doublet quark $Q^{(n)}$	$(1/6)g'$	1	B_μ
	g_2	$\sigma^a/2$	W^a_μ
	g_s	$\lambda^a/2$	g^a_μ

Lagrangian, f^{abc}_i is the structure constant of $SU(3)$ for gluon and that of $SU(2)$ for the W boson. As long as we use the KK number conserving Lagrangian, second KK particles are produced in pair due to the KK number conservation, and hence the production rates are suppressed due to their small phase spaces.

Next we discuss the KK number violating interactions. The KK number violating operators have been discussed in Ref. [9] taking into account only the gauge interactions. In addition, we include also contributions of Yukawa interactions. The effective Lagrangian for the KK number violating operators turns out to be

$$\mathcal{L}_{\rm vio} = \frac{x_i}{4}\left\{N_i(f)c_t + \left[9C_j(f) - \frac{23}{3}C_j(G)\delta_{ij} + \frac{n_j}{3}\delta_{ij}\right]c_j\right\}\bar{f}^{(0)}t^a_i\gamma^\mu P_{L(R)}f^{(0)}V^{(2)a}_{i\mu}, \quad (3)$$

$$c_j \equiv \frac{\sqrt{2}x_j^2}{16\pi^2}\log\frac{\Lambda^2}{\mu^2}, \qquad c_t \equiv \frac{\sqrt{2}y_t^2}{16\pi^2}\log\frac{\Lambda^2}{\mu^2}. \quad (4)$$

Here, y_t is the top Yukawa coupling constant, x_i, n_i, $C_i(f)$, $C_i(G)$, and t^a_i are listed in Table IV, and $N_i(f)$ is listed in Table V. Indices i, and j run over the SM gauge interactions

TABLE IV. Coefficient in the KK number violating operator in the effective Lagrangian [Eq. (3)]. g', g_2, an dg_s are $U(1)$, $SU(2)$, and $SU(3)$ gauge coupling constants, and Y_f is $U(1)$ hypercharge. σ^a and λ^a are Pauli and Gell-Mann matrices, respectively.

	$U(1)$	$SU(2)$	$SU(3)$
x_i	$g'Y_f$	g_2	g_s
n_i	1	2	0
$C_j(f)$	Y_f^2	3/4	4/3
$C_i(G)$	0	2	3
t^a_i	**1**	$\sigma^a/2$	$\lambda^a/2$

TABLE V. Coefficient $N(f)$ in the KK number violating operator in the effective Lagrangian [Eq. (3)]. Q_3 is the third generation $SU(2)$-doublet quark, and T is the $SU(2)$ singlet top quark.

	$Q^{(0)}_3Q^{(0)}_3\gamma^{(2)}$, $Q^{(0)}_3Q^{(0)}_3W^{(2)}$, $Q^{(0)}_3Q^{(0)}_3g^{(2)}$, $T^{(0)}T^{(0)}g^{(2)}$	$T^{(0)}T^{(0)}\gamma^{(2)}$	Other
$N(f)$	1	5	0

$U(1)$, $SU(2)$, and $SU(3)$, and summation over f is implicitly made. The renormalization scale is denoted by μ. Contribution $9C_j(f)$ comes from Figs. 1(a)–1(c), contribution $-(23/3)C_j(G)\delta_{ij}$ comes from Figs. 1(d)–1(f), and contribution $(n_j/3)\delta_{ij}$ comes from Figs. 1(g) and 1(h). Contribution $N_i(f)c_t$ comes from diagrams in Fig. 2.

B. Production processes of $\gamma^{(2)}$ and $Z^{(2)}$

We are now in a position to discuss the production processes of $\gamma^{(2)}$ and $Z^{(2)}$. At the LHC, $\gamma^{(2)}$ and $Z^{(2)}$ are produced through two type of processes: (1) direct productions and (2) indirect productions via the cascade decays of the second KK colored particles. The production cross sections of $\gamma^{(2)}$ and $Z^{(2)}$ have originally been calculated in Ref. [8], and their calculation includes all of the KK number conserving processes and the direct one-body production processes of the second KK gauge bosons. In this article, we calculate the production cross sections of $\gamma^{(2)}$ and $Z^{(2)}$ including all significant processes. For example, our calculation includes $pp \to q^{(2)}q^{(0)}$, $pp \to \gamma^{(2)}q^{(0)}$, $pp \to q^{(2)}\bar{q}^{(0)}$, and so on. Importantly, these processes provide large contributions to $\gamma^{(2)}$ and $Z^{(2)}$ productions, particularly for large $1/R$ ($\gtrsim 800$ GeV). We show the relevant processes to the $\gamma^{(2)}$ production in Figs. 3–8.

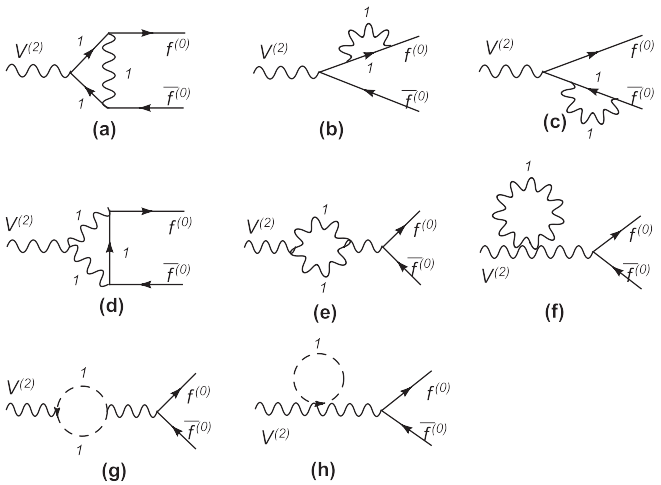


FIG. 1. The KK number violating vertices for $\bar{f}^{(0)}t^a\gamma^\mu P_{L(R)}f^{(0)}V^{(2)a}_{i\mu}$ induced from gauge interactions. The attached number represents the KK number of a KK particle in the loop.

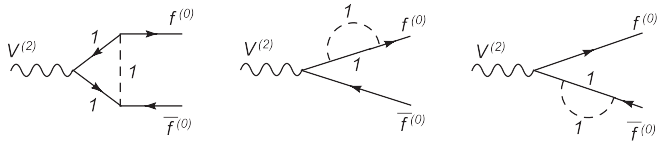


FIG. 2. The KK number violating vertices for $\bar{f}^{(0)} t^a \gamma^\mu P_{L(R)} f^{(0)} V^{(2)a}_{i\mu}$ induced from Yukawa interactions. The attached number represents the KK number of a KK particle in the loop.

Figure 3 (Fig. 6) shows the direct production of $\gamma^{(2)}$ through KK number conserving (violating) processes. Some of these processes also produce $q^{(2)}$, $\bar{q}^{(2)}$, and $g^{(2)}$, and they decay into $\gamma^{(2)}$ and $Z^{(2)}$. We must include those contributions in the calculation of the production cross section of $\gamma^{(2)}$ and $Z^{(2)}$. Figure 4 (Fig. 7) shows the production of $q^{(2)}$ and $\bar{q}^{(2)}$ through KK number conserving (violating) processes, and Fig. 5 (Fig. 8) shows the production of $g^{(2)}$ through KK number conserving (violating)

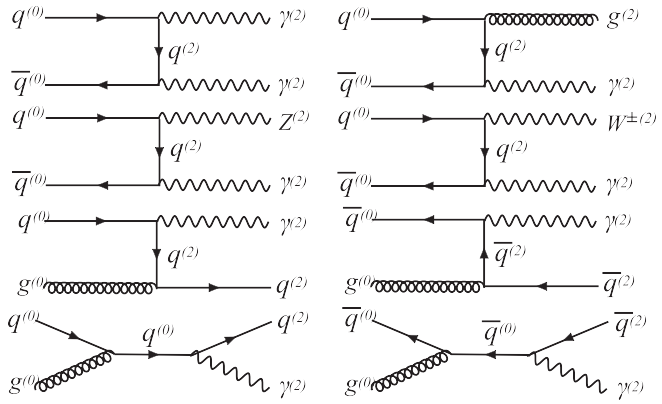


FIG. 3. The production of $\gamma^{(2)}$ through KK number conserving processes.

processes. These colored particles decay into $\gamma^{(2)}$ and $Z^{(2)}$. Here the gray circle in Figs. 6–8 stands for the KK number violating vertex. In the s-channel processes in Fig. 7, the contributions from $g^{(2)}$ one-body direct production are included, while the contributions from $\gamma^{(2)}$ one-body direct production are not included. Hence, $\gamma^{(2)}$ one-body direct production is shown in Fig. 6, and $g^{(2)}$ one-body direct production is not shown in Fig. 8. Note that the $\gamma^{(2)}$ production from the $Z^{(2)}$ decay can be neglected, because the branching ratio $Z^{(2)} \to L^{(2)}\bar{L}^{(0)} \to \gamma^{(2)} L^{(0)} \bar{L}^{(0)}$ is small enough. The processes of $Z^{(2)}$ production are almost the same as the $\gamma^{(2)}$ production, so we can skip the discussion of the $Z^{(2)}$ production. In Figs. 6 and 8, processes which have the final state $\gamma^{(2)}\gamma^{(0)}$, $\gamma^{(2)} g^{(0)}$, $g^{(2)}\gamma^{(0)}$, or $g^{(2)} g^{(0)}$ are not shown, because in this calculation, $\gamma^{(0)}$ and $g^{(0)}$ in these processes are the origin of the infrared divergences for the one-body production processes of second KK gauge bosons. The divergences can be removed by the calculation with a complete treatment.

In order to calculate the indirect production cross sections of $\gamma^{(2)}$ and $Z^{(2)}$, we calculate the branching ratio of $g^{(2)}$ and $q^{(2)}$. We show the branching ratio of the $SU(2)$ singlet KK down-type quark $D^{(2)}$ in Fig. 9, the branching ratio of the $SU(2)$ singlet KK up-type quark $U^{(2)}$ in Fig. 10, and the branching ratio of the $SU(2)$ doublet KK quark $Q^{(2)}$ in Fig. 11 as a function of $1/R$. Since $U^{(2)}$ and $D^{(2)}$ are $SU(2)$ singlet, they couple only with the $U(1)$ hypercharge gauge boson. Please note that the Weinberg angle of the neutral KK gauge boson is almost equal to 0 [9], and hence it is possible to identify the KK hypercharge gauge boson as the KK photon. Thus, as shown in Figs. 9 and 10, $D^{(2)}$ and $U^{(2)}$ decay into the KK photon, and $D^{(2)}$ and $U^{(2)}$ can be dominant sources of $\gamma^{(2)}$. On the other hand, $Q^{(2)}$ dominantly decays into $Z^{(2)}$, and hence $Q^{(2)}$ are dominant sources of $Z^{(2)}$.

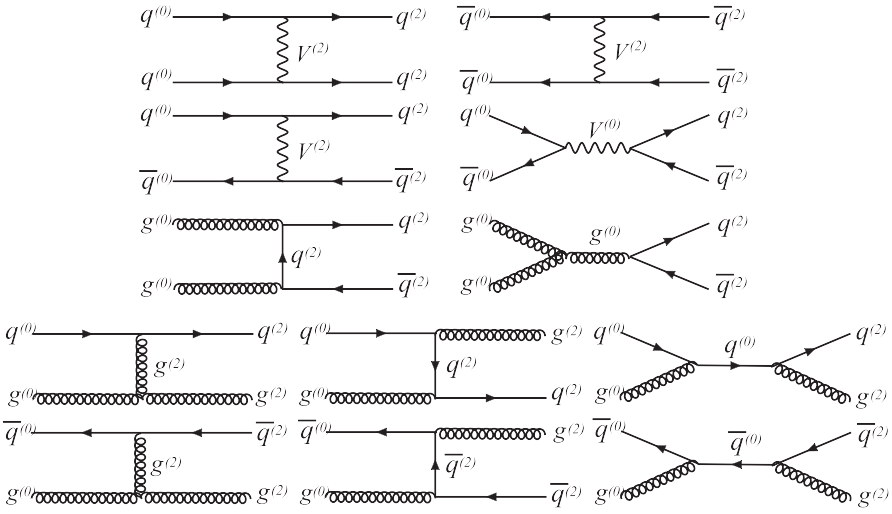


FIG. 4. The production of $q^{(2)}$ through KK number conserving processes. V stands for γ, $W^\pm$, Z, and g.

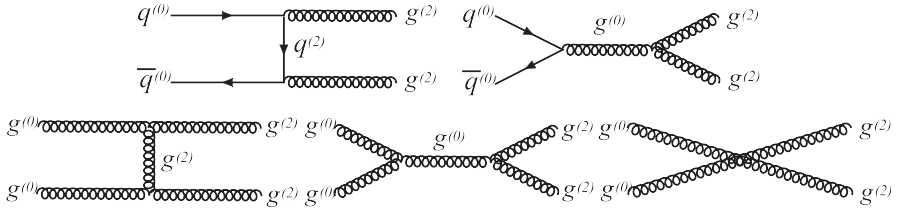


FIG. 5. The production of $g^{(2)}$ through KK number conserving processes.

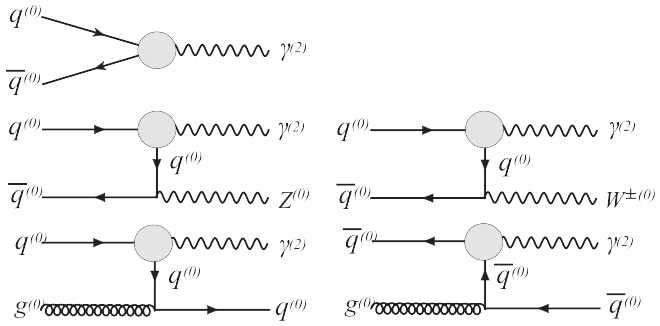


FIG. 6. The direct production of $\gamma^{(2)}$ through KK number violating processes. The gray circle represents the KK number violating vertex.

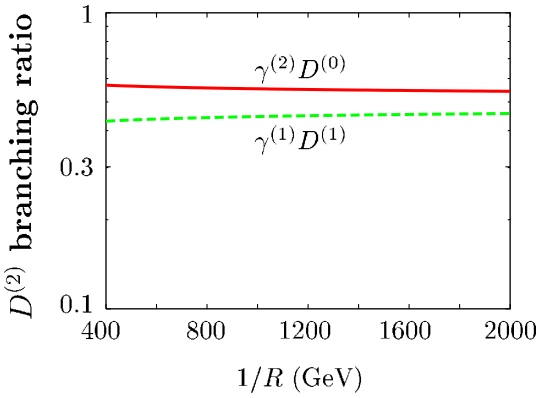


FIG. 9 (color online). The branching ratio of $D^{(2)}$.

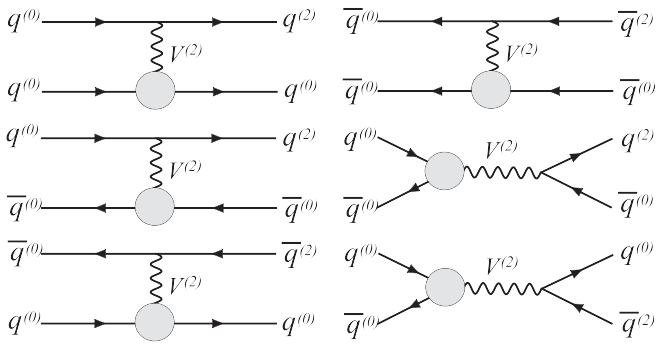


FIG. 7. The production of $q^{(2)}$ through KK number violating processes. $V^{(2)}$ stands for $\gamma^{(2)}$, $W^{\pm(2)}$, $Z^{(2)}$, and $g^{(2)}$. The gray circle represents the KK number violating vertex.

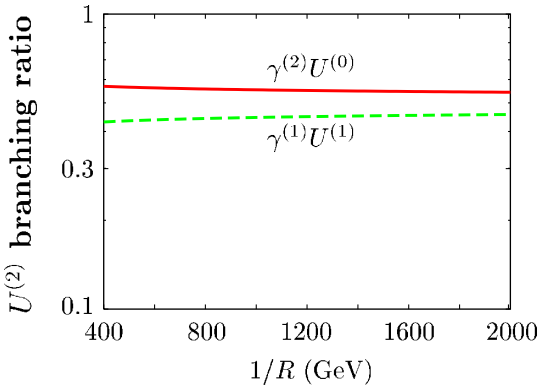


FIG. 10 (color online). The branching ratio of $U^{(2)}$.

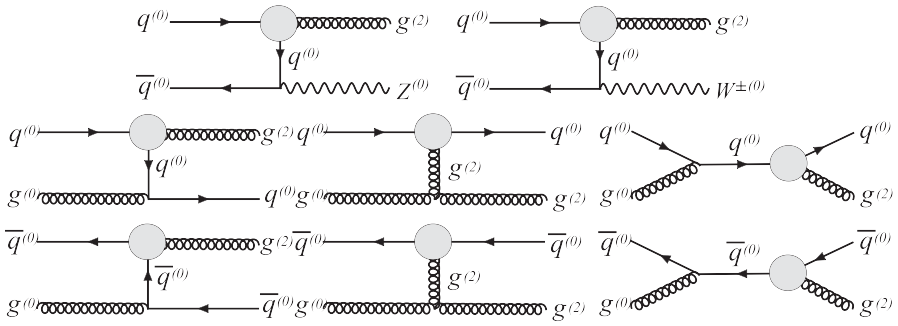


FIG. 8. The production of $g^{(2)}$ through KK number violating processes. The gray circle represents the KK number violating vertex.

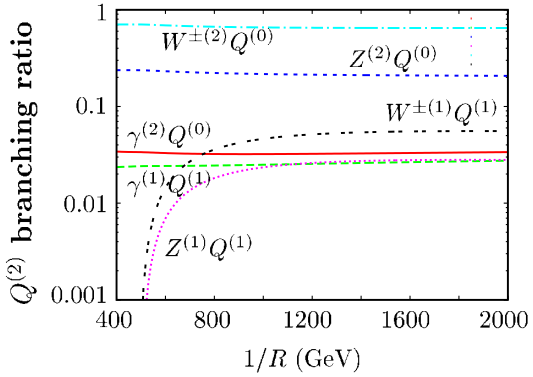


FIG. 11 (color online). The branching ratio of $Q^{(2)}$.

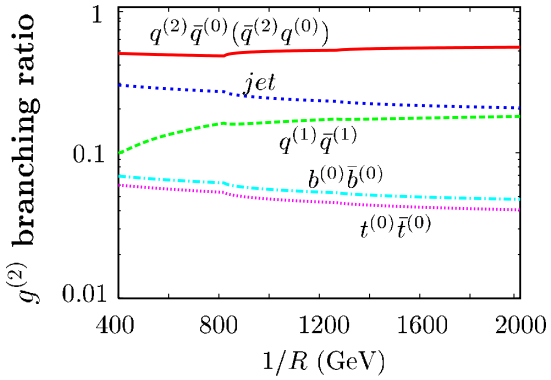


FIG. 12 (color online). The branching ratio of $g^{(2)}$.

Finally, we show the branching ratio of $g^{(2)}$ in Fig. 12. In this figure, generation indices are implicitly summed for each line, while *jet* represents the sum of first and second generation SM quarks. At the LHC, the production rates of the second KK colored particles are much larger than those of other second KK particles, and $g^{(2)}$ and $q^{(2)}$ dominantly decay into a second KK particle and a SM particle, as shown in these figures. Hence, the indirect productions of $\gamma^{(2)}$ and $Z^{(2)}$ from their cascade decays are quite significant. Note that the branching ratios of each second KK particle calculated in this work are different from that in Ref. [8] due to two reasons. The one is the difference of the KK number violating operators. In particular, we include the KK number violating operators induced by the top Yukawa coupling. The other is the difference of mass spectrum of KK particles. By comparing our mass spectrum (Table II) with theirs (Fig. 1 in Ref. [8]), we find the difference in these mass spectra. The difference of the branching ratios from the previous work [8] mainly arises from the latter reason. In the next section, we will calculate the production rates of $\gamma^{(2)}$ and $Z^{(2)}$ using the results in this section.

IV. NUMERICAL RESULTS

In this section, we present numerical results of the cross sections for $\gamma^{(2)}$ and $Z^{(2)}$ productions and estimate the number of the dilepton signal from $\gamma^{(2)}$ and $Z^{(2)}$ decays at the LHC. The calculations of the cross sections have been performed by using the CALCHEP [13] implementing the Lagrangian Eq. (3) derived in the previous section.

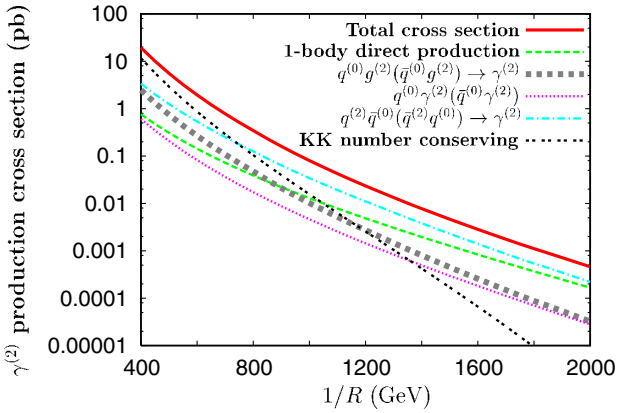


FIG. 13 (color online). The production cross sections of $\gamma^{(2)}$. The red solid line shows the total cross section, and other lines show the production cross sections of $\gamma^{(2)}$ for each process as denoted in the legend.

In Fig. 13 (Fig. 14), we show the production cross section of $\gamma^{(2)}$ ($Z^{(2)}$) as a function of $1/R$. In the calculation, we have used the CTEQ6L code [14] as a parton distribution function (PDF). The red solid line shows the total cross section of $\gamma^{(2)}$ ($Z^{(2)}$) production. Note that, although we show the results for only significant processes in these figures and discuss them, all processes shown in Figs. 3–8 are included in the calculation of the total cross section. As shown in these figures, for large $1/R$ ($\gtrsim$ 800 GeV), the KK number violating processes dominantly contribute to the total production cross section. This means that the KK number violating operators are important for the discrimination of the MUED model from other TeV scale models.

We discuss the significance of each production process. (i) For large $1/R$ ($1/R \gtrsim 800$ GeV), one-body direct pro-

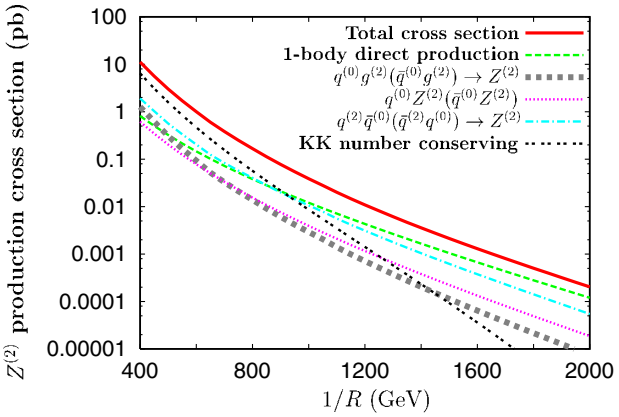


FIG. 14 (color online). The production cross sections of $Z^{(2)}$. The red solid line shows the total cross section, and other lines show the production cross sections of $Z^{(2)}$ for each process as denoted in the legend.

duction processes are important, because even if $\gamma^{(2)}$ and $Z^{(2)}$ are too heavy to be produced in pair, these processes provide $\gamma^{(2)}$ and $Z^{(2)}$ efficiently. (ii) In addition to evading the suppression of small phase space, the processes $pp \to q^{(0)}V^{(2)}(\bar{q}^{(0)}V^{(2)})$ have notable features. Since the PDF of proton is dominated by gluons and the valence quarks, i.e., up and down quarks, the rate of $q^{(0)}g^{(0)}$ collision is larger than $q^{(0)}\bar{q}^{(0)}$ collision. Furthermore, the cross section of these processes has the large logarithm factor:

$$\sigma \sim \log\left[\frac{(s - m_{V2}^2) + m_{q0}^2}{m_{q0}^2}\right]. \tag{5}$$

Here m_{q0} is the mass of a SM quark, m_{V2} is the mass of the second KK gauge boson, and s is the square of the initial state total energy. In usual cases, cross sections decrease according to the increasing of $1/R$ and s. However, this logarithm factor prevents the drastic decreasing. Thus, in all ranges of $1/R$ in these figures, indirect productions of $\gamma^{(2)}$ and $Z^{(2)}$ from $pp \to q^{(0)}g^{(2)}(\bar{q}^{(0)}g^{(2)})$ and direct productions $pp \to q^{(0)}\gamma^{(2)}(\bar{q}^{(0)}\gamma^{(2)})$ or $pp \to q^{(0)}Z^{(2)}(\bar{q}^{(0)}Z^{(2)})$ provide a non-negligible contribution to their production cross sections. (iii) At the LHC, the final state $q^{(2)}\bar{q}^{(0)}$ (or $\bar{q}^{(2)}q^{(0)}$) is mostly provided by the s-channel process mediated by the $g^{(2)}$ propagator. In other words, these include the contributions from $g^{(2)}$ one-body production and indirect productions through the cascade decay of $g^{(2)}$. In this case, the pole resonance of $g^{(2)}$ leads the large enhancement of the cross section. Thus the processes $pp \to q^{(2)}\bar{q}^{(0)}(\bar{q}^{(2)}q^{(0)})$ have large cross sections, even if $1/R$ is rather large, and provide large contributions to the indirect productions of $\gamma^{(2)}$ and $Z^{(2)}$. (iv) For small $1/R$ ($\lesssim$ 800 GeV), the cross sections of KK number conserving processes are larger than those of KK number violating processes, because the KK number conserving operators have no loop suppressions. However, for large $1/R$ ($\gtrsim$ 800 GeV), the contribution from KK number conserving processes decreases rapidly because of the severe kinematical suppression on the pair production of the second KK particles.

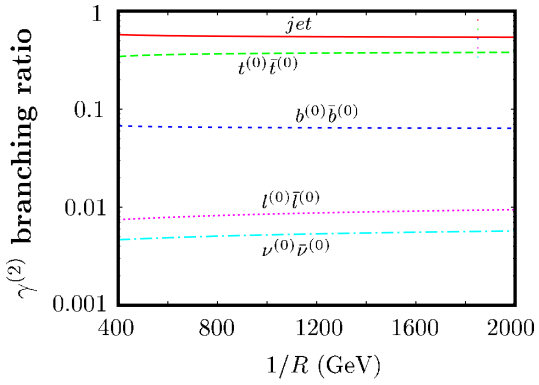


FIG. 15 (color online). The branching ratio of $\gamma^{(2)}$.

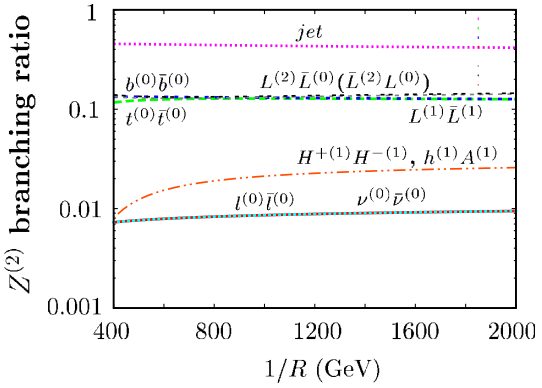


FIG. 16 (color online). The branching ratio of $Z^{(2)}$.

TABLE VI. The number of the dilepton signals at the LHC with 100 fb^{-1}.

$1/R$	Dileptons from $\gamma^{(2)}$	Dileptons from $Z^{(2)}$
400 GeV	1.5×10^4	9.4×10^3
800 GeV	2.9×10^2	1.6×10^2
1200 GeV	2.1×10	1.2×10
1600 GeV	2.6	1.4
2000 GeV	4.4×10^{-1}	2.3×10^{-1}

Assuming an integrated luminosity of 100 fb^{-1}, the number of produced $\gamma^{(2)}$ and $Z^{(2)}$ are calculated as 10^6–10^2 for 400 GeV $\leq 1/R \leq$ 2000 GeV. Once $\gamma^{(2)}$ and $Z^{(2)}$ are produced, they decay into dileptons with non-zero branching ratios. In order to estimate the number of dilepton signals from $\gamma^{(2)}$ and $Z^{(2)}$, we calculate these branching ratios. Figure 15 (Fig. 16) shows the branching ratio of $\gamma^{(2)}$ ($Z^{(2)}$). In both figures, each line generation indices is implicitly summed. $\gamma^{(2)}$ is the lightest second KK particle, and the masses of the first KK fermions are always heavier than half of the $\gamma^{(2)}$ mass. Then $\gamma^{(2)}$ must decay into a SM fermion pair through KK number violating processes. On the other hand, $Z^{(2)}$ has many decay channels comparing with $\gamma^{(2)}$. Although the decay channels of $\gamma^{(2)}$ and $Z^{(2)}$ are quite different with each other, coincidentally the branching ratio to dilepton is almost the same.

In Table VI, we show the number of the dilepton signals assuming the luminosity 100 fb^{-1}. Table VI shows that for $1/R \lesssim$ 1600 GeV it remains possible that we can discriminate the MUED model from other models by using the dilepton signals with 100 fb^{-1} integrated luminosity. If the MUED model is realized by the nature, in addition to the dilepton signals from the decay of $\gamma^{(2)}$ and $Z^{(2)}$, many new particles with degenerate mass spectrum around $1/R$ (i.e., the first KK particles) are discovered. Connecting the observational results of dilepton signals and the discovery of the first KK particles, it is possible to confirm the MUED model. In this work, we do not discuss the feasibility of the MUED model confirmation, which needs a complete analysis with Monte Carlo simulation. It is beyond the scope of this paper. This will be addressed in future work [15].

V. SUMMARY

At the LHC, the discrimination of the MUED model from other models is difficult, because the signals of new particles of TeV scale models are quite similar to each other. For the discrimination, we focused on a distinct feature of the MUED model, i.e., the existence of the KK tower. Once $\gamma^{(2)}$ and $Z^{(2)}$ are produced, they can decay into dilepton which provides a very clear signal of the second KK particles. The discovery of the second KK particles strongly indicates the existence of the KK tower and consequently will lead to the confirmation of the MUED model. In order to estimate the number of the dilepton events from $\gamma^{(2)}$ and $Z^{(2)}$, we have calculated the production rates of $\gamma^{(2)}$ and $Z^{(2)}$ at the LHC.

First we have calculated the KK number violating operators. They play a crucial role for the discrimination, because $\gamma^{(2)}$ and $Z^{(2)}$ can decay into dilepton through these couplings. In the calculation, we have included the contribution of the top Yukawa coupling to improve the KK number violating operators. This has improved the branching ratio calculations of the second KK gauge bosons. Next we have shown all significant processes for $\gamma^{(2)}$ and $Z^{(2)}$ productions including both the KK number conserving and violating interactions. Then we have calculated the production cross sections of $\gamma^{(2)}$ and $Z^{(2)}$. Finally we have found that $\mathcal{O}(10^6)$–$\mathcal{O}(10^2)$ of $\gamma^{(2)}$ and $Z^{(2)}$ production events are expected for $400\,\mathrm{GeV} \leq 1/R \leq 2000\,\mathrm{GeV}$ with an integrated luminosity of $100\,\mathrm{fb}^{-1}$. We have also discussed the significance of various production processes and found that the KK number violating processes give leading contributions to the $\gamma^{(2)}$ and $Z^{(2)}$ productions for $1/R \gtrsim 800\,\mathrm{GeV}$. In particular, our original processes (for example, $pp \to q^{(2)}q^{(0)}$, $pp \to q^{(2)}\bar{q}^{(0)}$, and so on) have provided large contributions to the $\gamma^{(2)}$ and $Z^{(2)}$ productions, and hence they have notable significance for the discrimination.

As a result of the calculations, we have shown the expected production number of dileptons from the $\gamma^{(2)}$ and $Z^{(2)}$ decays (Table VI). We have found that for $1/R \lesssim 1600$ GeV there is a chance to discriminate models by using the dilepton signals with $100\ \mathrm{fb}^{-1}$ integrated luminosity. For the discrimination, it is crucial whether the dilepton signals can be observed or not. We need further study to discuss the feasibility of the discovery of the MUED model by estimating the background from the SM.

In addition, as discussed in Ref. [16], when $1/R$ is not so large, the bump hunting for $g^{(2)}$ in the dijet invariant mass distribution might be one of the useful ideas for the complementary check of the discrimination by the dilepton signals.[3] However, since jet analysis is accompanied with SM QCD background, precise simulation is necessary for the bump hunting for $g^{(2)}$. We leave those for future work [15].

[3]Note that the simulation result of the $g^{(2)}$ invariant mass distribution of the dijet signal shown in Ref. [16] cannot apply for the MUED model, because the coefficient of the KK number violating operator in their framework is different from the MUED model.

ACKNOWLEDGMENTS

The work of J. S. was supported in part by the Grant-in-Aid for the Ministry of Education, Culture, Sports, Science, and Technology, Government of Japan (No. 20025001, No. 20039001, and No. 20540251). The work of M. Y. was supported in part by the Grant-in-Aid for the Ministry of Education, Culture, Sports, Science, and Technology, Government of Japan (No. 20007555).

APPENDIX: DECAY RATES OF SECOND KK PARTICLES

In this Appendix we show analytic expressions for decay rates of second KK particles. The branching ratios of them (Fig. 9–12, 15, and 16) are obtained by using the following expressions. The decay rate of the second KK gauge boson $V^{(2)}$ is given by

$$\Gamma_{V^{(2)}\to f^{(2)}\bar{f}^{(0)}} = \frac{C_{220}}{96\pi} m_{V2} \sqrt{\left(1 - \frac{m_{f2}^2 + m_{f0}^2}{m_{V2}^2}\right)^2 - 4\frac{m_{f2}^2 m_{f0}^2}{m_{V2}^4}} \times \left[1 - \frac{m_{f2}^2 + m_{f0}^2}{m_{V2}^2} + \left(1 + \frac{m_{f2}^2 - m_{f0}^2}{m_{V2}^2}\right) \times \left(1 - \frac{m_{f2}^2 - m_{f0}^2}{m_{V2}^2}\right) + \alpha \frac{m_{f2} m_{f0}}{m_{V2}^2}\right], \quad \text{(A1)}$$

$$\Gamma_{V^{(2)}\to f^{(1)}\bar{f}^{(1)}} = \frac{C_{211}}{48\pi} m_{V2} \left[1 - \frac{4m_{f1}^2}{m_{V2}^2}\right]^{3/2}, \quad \text{(A2)}$$

$$\Gamma_{V^{(2)}\to f^{(0)}\bar{f}^{(0)}} = \frac{m_{V2}}{24576\pi} \sqrt{1 - 4\frac{m_{f0}^2}{m_{V2}^2}} \left[C_{200}\left(1 + \frac{2m_{f0}^2}{m_{V2}^2}\right) + C'_{200}\left(1 - \frac{4m_{f0}^2}{m_{V2}^2}\right)\right], \quad \text{(A3)}$$

$$\Gamma_{Z^{(2)}\to h^{(1)}A^{(1)}} = \Gamma_{Z^{(2)}\to H^{+(1)}H^{-(1)}} = \frac{g_2^2}{384\pi} m_{Z2} \sqrt{\left(1 - \frac{m_{H1}^2 + m_{H2}^2}{m_{Z2}^2}\right)^2 - 4\frac{m_{H1}^2 m_{H2}^2}{m_{Z2}^4}} \times \left[2\left(1 - \frac{m_{H1}^2 + m_{H2}^2}{m_{Z2}^2}\right) - \left(1 + \frac{m_{H1}^2 - m_{H2}^2}{m_{Z2}^2}\right) \times \left(1 - \frac{m_{H1}^2 - m_{H2}^2}{m_{Z2}^2}\right)\right]. \quad \text{(A4)}$$

Here m_{V2}, m_{f2}, m_{f1}, and m_{f0} are the masses of $V^{(2)}$, the second KK fermion $f^{(2)}$, the first KK fermion $f^{(1)}$, and the SM fermion $f^{(0)}$. For $V^{(2)} = g^{(2)}$, $C_{220} = C_{211} = g_s^2$. For $V^{(2)} = Z^{(2)}$, $C_{200} = C_{211} = g_2^2/2$. C_{200}, and C'_{200} are listed

TABLE VII. Coefficients C_{200} and C'_{200} in Eq. (A3). Here c', c_2, c_s, and c_t are given in Eq. (4).

Process	C_{200}	C'_{200}
$\gamma^{(2)} \to e^{(0)}\bar{e}^{(0)}$	$(g'^2/2)[85c' + 27c_2]^2$	$(g'^2/2)[(193/3)c' - 27c_2]^2$
$\gamma^{(2)} \to \nu^{(0)}\bar{\nu}^{(0)}$	$(g'^2/2)[(31/3)c' + 27c_2]^2$	$(g'^2/2)[(31/3)c' + 27c_2]^2$
$\gamma^{(2)} \to u^{(0)}\bar{u}^{(0)}$	$(g'^2/6) \times [215c' + 81c_2 + 720c_s]^2$	$(g'^2/2) \times [67c' - 27c_2 + 144c_s]^2$
$\gamma^{(2)} \to d^{(0)}\bar{d}^{(0)}$	$(g'^2/6) \times [25c' - 81c_2 + 144c_s]^2$	$(g'^2/2) \times [13c' + 27c_2 + 144c_s]^2$
$\gamma^{(2)} \to t^{(0)}\bar{t}^{(0)}$	$(g'^2/6) \times [215c' + 81c_2 + 720c_s + 252c_t]^2$	$(g'^2/2) \times [67c' - 27c_2 + 144c_s + 76c_t]^2$
$\gamma^{(2)} \to b^{(0)}\bar{b}^{(0)}$	$(g'^2/6) \times [25c' - 81c_2 + 144c_s - 12c_t]^2$	$(g'^2/2) \times [13c' + 27c_2 + 144c_s + 4c_t]^2$
$Z^{(2)} \to e^{(0)}\bar{e}^{(0)}$	$(g_2^2/18)[27c' - 95c_2]^2$	$(g_2^2/18)[27c' - 95c_2]^2$
$Z^{(2)} \to \nu^{(0)}\bar{\nu}^{(0)}$	$(g_2^2/18)[27c' - 95c_2]^2$	$(g_2^2/18)[27c' - 95c_2]^2$
$Z^{(2)} \to u^{(0)}\bar{u}^{(0)}$	$(g_2^2/6)[3c' - 95c_2 + 144c_s]^2$	$(g_2^2/6)[3c' - 95c_2 + 144c_s]^2$
$Z^{(2)} \to d^{(0)}\bar{d}^{(0)}$	$(g_2^2/6)[3c' - 95c_2 + 144c_s]^2$	$(g_2^2/6)[3c' - 95c_2 + 144c_s]^2$
$Z^{(2)} \to t^{(0)}\bar{t}^{(0)}$	$(g_2^2/6) \times [3c' - 95c_2 + 144c_s + 12c_t]^2$	$(g_2^2/6) \times [3c' - 95c_2 + 144c_s + 12c_t]^2$
$Z^{(2)} \to b^{(0)}\bar{b}^{(0)}$	$(g_2^2/6) \times [3c' - 95c_2 + 144c_s + 12c_t]^2$	$(g_2^2/6) \times [3c' - 95c_2 + 144c_s + 12c_t]^2$
$g^{(2)} \to u^{(0)}\bar{u}^{(0)}$	$g_s^2[17c' + 27c_2 - 88c_s]^2$	$g_s^2[15c' - 27c_2]^2$
$g^{(2)} \to d^{(0)}\bar{d}^{(0)}$	$g_s^2[5c' + 27c_2 - 88c_s]^2$	$g_s^2[3c' - 27c_2]^2$
$g^{(2)} \to t^{(0)}\bar{t}^{(0)}$	$g_s^2[17c' + 27c_2 - 88c_s + 8c_t]^2$	$g_s^2[15c' - 27c_2]^2$
$g^{(2)} \to b^{(0)}\bar{b}^{(0)}$	$g_s^2[5c' + 27c_2 - 88c_s + 4c_t]^2$	$g_s^2[3c' - 27c_2 - 4c_t]^2$

in Table VII. The coefficient α depends on the mixing between the mass eigenstate and the interaction eigenstate of the KK fermions. The mixing is negligible except for the KK top quark, and hence α is as follows:

$$\alpha = \frac{12m_t}{\sqrt{(\tilde{m}_{T^{(2)}} + \tilde{m}_{t^{(2)}})^2 + 4m_t^2}} \quad \text{for } f^{(2)} = T^{(2)}$$
$$\alpha = \frac{-12m_t}{\sqrt{(\tilde{m}_{T^{(2)}} + \tilde{m}_{t^{(2)}})^2 + 4m_t^2}} \quad \text{for } f^{(2)} = t^{(2)} \tag{A5}$$
$$\alpha = 0 \quad \text{for } f^{(2)} = \text{other second KK fermions.}$$

Here m_t stands for the SM top quark mass, and $\tilde{m}_{T^{(2)}}$ and $\tilde{m}_{t^{(2)}}$ are given by

$$\tilde{m}_{T^{(2)}} = \frac{2}{R} + \frac{2}{R}\left[3\frac{g_s^2}{16\pi^2} + \frac{g'^2}{16\pi^2}\right]\ln\frac{\Lambda^2}{\mu^2} + \frac{2}{R}\left[-\frac{3}{2}\frac{y_t^2}{16\pi^2}\right]\ln\frac{\Lambda^2}{\mu^2}$$
$$\tilde{m}_{t^{(2)}} = \frac{2}{R} + \frac{2}{R}\left[3\frac{g_s^2}{16\pi^2} + \frac{27}{16}\frac{g_2^2}{16\pi^2} + \frac{1}{16}\frac{g'^2}{16\pi^2}\right]\ln\frac{\Lambda^2}{\mu^2} + \frac{2}{R}\left[-\frac{3}{4}\frac{y_t^2}{16\pi^2}\right]\ln\frac{\Lambda^2}{\mu^2}. \tag{A6}$$

The decay rate of the first and second generation second KK quarks are given by

$$\Gamma_{q^{(2)}\to V^{(2)}q^{(0)}} = \frac{K}{16\pi}m_{q2}\sqrt{\left(1 - \frac{m_{V2}^2 + m_{q0}^2}{m_{q2}^2}\right)^2 - 4\frac{m_{V2}^2 m_{q0}^2}{m_{q2}^4}} \times \left[1 - \frac{m_{V2}^2 - m_{q0}^2}{m_{q2}^2} + \left(1 + \frac{m_{q2}^2 - m_{q0}^2}{m_{V2}^2}\right) \times \left(1 - \frac{m_{V2}^2 + m_{q0}^2}{m_{q2}^2}\right)\right], \tag{A7}$$

$$\Gamma_{q^{(2)}\to V^{(1)}q^{(1)}} = \frac{K}{16\pi}m_{q2}\sqrt{\left(1 - \frac{m_{V1}^2 + m_{q1}^2}{m_{q2}^2}\right)^2 - 4\frac{m_{V1}^2 m_{q1}^2}{m_{q2}^4}} \times \left[1 + \frac{m_{q1}^2 - m_{V1}^2}{m_{q2}^2} - 6\frac{m_{q1}}{m_{q2}} + \left(1 + \frac{m_{q2}^2 - m_{q1}^2}{m_{V2}^2}\right)\left(1 - \frac{m_{V2}^2 + m_{q1}^2}{m_{q2}^2}\right)\right]. \tag{A8}$$

Here m_{q2}, m_{q1}, and m_{q0} are the masses of $q^{(2)}$, $q^{(1)}$, and $q^{(0)}$. $K = g'^2/72$ for $(q, V) = (Q, \gamma)$, $K = g_2^2/4$ for $(q, V) = (Q, W^{\pm})$, $K = g_2^2/8$ for $(q, V) = (Q, Z)$, $K = 2g'^2/9$ for $(q, V) = (U, \gamma)$, and $K = g'^2/18$ for $(q, V) = (D, \gamma)$.

[1] T. Appelquist, H. C. Cheng, and B. A. Dobrescu, Phys. Rev. D **64**, 035002 (2001).
[2] I. Antoniadis, Phys. Lett. B **246**, 377 (1990).
[3] H. C. Cheng, J. L. Feng, and K. T. Matchev, Phys. Rev. Lett. **89**, 211301 (2002); G. Servant and T. M. P. Tait, Nucl. Phys. **B650**, 391 (2003).

[4] B. A. Dobrescu and E. Poppitz, Phys. Rev. Lett. **87**, 031801 (2001).
[5] S. Matsumoto, J. Sato, M. Senami, and M. Yamanaka, Phys. Lett. B **647**, 466 (2007).
[6] K. Agashe, N. G. Deshpande, and G. H. Wu, Phys. Lett. B **511**, 85 (2001); **514**, 309 (2001); T. Appelquist and B. A. Dobrescu, Phys. Lett. B **516**, 85 (2001); T. Appelquist and H. U. Yee, Phys. Rev. D **67**, 055002 (2003); J. F. Oliver, J. Papavassiliou, and A. Santamaria, Phys. Rev. D **67**, 056002 (2003); D. Chakraverty, K. Huitu, and A. Kundu, Phys. Lett. B **558**, 173 (2003); A. J. Buras, M. Spranger, and A. Weiler, Nucl. Phys. **B660**, 225 (2003); P. Colangelo, F. De Fazio, R. Ferrandes, and T. N. Pham, Phys. Rev. D **73**, 115006 (2006); I. Gogoladze and C. Macesanu, Phys. Rev. D **74**, 093012 (2006).
[7] M. Kakizaki, S. Matsumoto, Y. Sato, and M. Senami, Phys. Rev. D **71**, 123522 (2005); S. Matsumoto and M. Senami, Phys. Lett. B **633**, 671 (2006); F. Burnell and G. D. Kribs, Phys. Rev. D **73**, 015001 (2006); M. Kakizaki, S. Matsumoto, and M. Senami, Phys. Rev. D **74**, 023504 (2006); K. Kong and K. T. Matchev, J. High Energy Phys. 01 (2006) 038; S. Matsumoto, J. Sato, M. Senami, and M. Yamanaka, Phys. Rev. D **76**, 043528 (2007).
[8] A. Datta, K. Kong, and K. T. Matchev, Phys. Rev. D **72**, 096006 (2005); **72**, 119901(E) (2005).
[9] H. C. Cheng, K. T. Matchev, and M. Schmaltz, Phys. Rev. D **66**, 036005 (2002).
[10] G. Bhattacharyya, A. Datta, S. K. Majee, and A. Raychaudhuri, Nucl. Phys. **B760**, 117 (2007).
[11] A. J. Barr, Phys. Lett. B **596**, 205 (2004).
[12] G. H. Brooijmans *et al.*, arXiv:0802.3715.
[13] A. Pukhov, arXiv:hep-ph/0412191.
[14] J. Pumplin, D. R. Stump, J. Huston, H. L. Lai, P. Nadolsky, and W. K. Tung, J. High Energy Phys. 07 (2002) 012.
[15] S. Matsumoto, J. Sato, M. Senami, and M. Yamanaka (work in progress).
[16] S. C. Park and J. Shu, Phys. Rev. D **79**, 091702(R) (2009).